JOURNAL OF AIRCRAFT
Vol. 38, No. 6, November–December 2001

Aeroelastic Deformation Measurements of Flap, Gap, and Overhang on a Semispan Model

A. W. Burner* and Tianshu Liu†
NASA Langley Research Center, Hampton, Virginia 23681-2199
Sanjay Garg‡
High Technology Corporation, Hampton, Virginia 23666
Terence A. Ghee§
Naval Air Systems Command, Patuxent River, Maryland 20670-1906
and
Nigel J. Taylor¶
Defense Evaluation and Research Agency Farnborough, Farnborough Hampshire, England GU 14 OLX, United Kingdom

Single-camera, single-view videogrammetry has been used for the first time to determine static aeroelastic deformation of a slotted flap configuration on a semispan model at the National Transonic Facility (NTF). Deformation was determined by comparing wind-off to wind-on spatial data from targets placed on the main element, shroud, and flap of the model. Digitized video images from a camera were recorded and processed to determine automatically target image plane locations that were then corrected for sensor, lens, and frame grabber spatial errors. The videogrammetric technique used for the measurements presented here has been established at NASA facilities as the technique of choice when high-volume static aeroelastic data with minimum impact on data taking are required. However, the primary measurement at the NTF with this technique in the past has been the measurement of the static aeroelastic wing twist of the main wing element on full span models rather than for the measurement of component deformation. Considerations for using the videogrammetric technique for semispan component deformation measurements as well as representative results are presented.

Nomenclature

c	=	chord length
L	=	displacement magnitude in X, Z plane
Q	=	dynamic pressure
X	=	streamwise coordinate in object space
Y	=	crossflow coordinate in object space
Z	=	vertical coordinate in object space
α	=	geometrical angle-of-attack
Δgap	=	change in gap spacing due to aerodynamic loading
ΔOH	=	change in overhang spacing due to aerodynamic loading
ΔX	=	displacement magnitude of streamwise coordinate
ΔY	=	displacement magnitude of crossflow coordinate
ΔZ	=	displacement magnitude of vertical coordinate
η	=	normalized semispan
θ	=	change in wing twist due to aerodynamic loading
ϕ	=	angle of displacement vector

Subscripts

n	=	target number, 1,2 (inboard reference); 3 (shroud); 4 [fore trailing-edge flap (TEF)]; 5 (aft TEF)
o	=	interpolated wind-off X value

Introduction

ON modern military air vehicles, high-lift systems are used to improve takeoff and landing performance. For naval air vehicles, an improvement in the lift coefficient in a landing or approach configuration allows for arrested landings at reduced speeds and/or increased payloads. In addition, reduced landing speeds reduce stress on the airframe. For conventional takeoff or landing, improved lift-to-drag ratios allow for shorter takeoff runs and/or greater payload capacity. For these reasons, it is imperative to quantify and improve the performance of high-lift systems, including trailing-edge flap (TEF), gap, and shroud geometry.

An effort has been initiated to develop procedures using the videogrammetric model deformation (VMD) measurement technique to measure TEF gap and flap and shroud geometry changes induced by aerodynamic loading. VMD measurement technique development with multiple cameras was initiated in the 1980s,[1] based on earlier successful wind-tunnel tests conducted in the 1970s using film cameras.[2] The introduction of image processing routines coupled with the development of a simplified single-camera, single-view photogrammetric technique permitted automated data acquisition and reduction. These developments facilitated use of the technique in production wind tunnels with very little negative impact on test schedule.[3] The target-tracking version of VMD developed under NASA contract and used for this test is discussed in

Presented as Paper 2000-2386 at the 21st AIAA Aerodynamic Measurement Technology and Ground Testing Conference, 19–22 June 2000; received 5 October 2000; revision received 18 January 2001; accepted for publication 2 February 2001.

*Research Scientist, Instrumentation Systems Development Branch, MS 236; a.w.burner@larc.nasa.gov. Senior Member AIAA.

†Research Scientist, Model Systems Branch, MS 238; t.liu@larc.nasa.gov. Member AIAA.

‡Research Scientist; currently Research Scientist, Advanced Systems Department, Hypertherm, Inc., Etna Road, Hanover, NH 03755; sanjay.garg@hypertherm.com.

§Aerodynamicist, Code 4321, Advanced Aerodynamics Branch, Building 2187, Suite 1320B; gheeta@navair.navy.mil. Senior Member AIAA.

¶Senior Scientist, Aero-Structures Department; currently Principal Aerodynamicist, Matra Bae Dynamics (U.K.) Ltd., FPC 460, P.O. Box 5, Filton, Bristol, England BS34 7QW, U.K.; nigel-j-taylor@bae.co.uk. Member AIAA.

Ref. 4. A review of the VMD measurement technique can be found in Ref. 5.

Component deformation measurements are especially troublesome due to difficulty in imaging the area of interest, limited target placement options, and the need to measure small deformation levels that are very sensitive to small errors in pitch angle (dependent on the radius from the center of rotation of the model). Although a few preliminary tests have been conducted during which flap angle changes with flow were measured at other noncryogenic facilities,[6] this paper will address the first application of the technique at the National Transonic Facility (NTF) for the combined measurement of TEF and shroud geometry changes under aerodynamic loading. In addition, this was the first application of the technique at the NTF with a semispan model and the first optical measurements of component deformation at the facility. Deformation measurements, including the deformation of control surfaces and associated components, are of particular importance in high Reynolds number facilities such as the NTF because high dynamic pressures Q, with accompanying deformation, are typically associated with high Reynolds number testing. For computational fluid dynamics (CFD) evaluation, it is important to quantify the gap and overhang differences from the static condition due to shroud and/or TEF deflections under load.

Because the intent of this paper is not to present extensive data on gap and flap deformation, only representative data will be presented. Rather, this paper relates experiences using videogrammetry in a large production wind tunnel for such measurements to aid potential users of the technique at the NTF and other facilities. Issues related to targeting such as location, application, contrast, surface quality, and target thickness will be addressed. Camera installation will be described along with initial camera calibration to establish camera calibration coefficients and camera location in the test-section coordinate system. A major concern for high-productivity facilities is that calibration time be kept to a minimum so as not to impact negatively productivity. Techniques employed to reduce significantly tunnel downtime for calibration will be described. The data acquisition procedure and interaction with the facility data acquisition system will be described. The advantages and disadvantages of a commercial prototype target-tracking image acquisition system will be discussed. The data reduction procedure to determine gap and flap deformation due to aerodynamic loading will also be described. The relation of centroid repeatability to the precision of the measurements will be addressed, along with estimates of uncertainty.

Technique

The VMD measurement technique consists of a single-camera, single-view, photogrammetric solution from digital images of targets placed on the wing at known semispan locations. Because only one camera is required, lighting requirements are reduced, which is especially advantageous when using existing test-section illumination. The technique is nonintrusive except for the targets, which may have some minor local effects on the aerodynamic data.[3] The basic hardware consists of a standard video-rate charge-coupled device (CCD) video camera, a frame grabber board, and a computer with image acquisition and reduction software. A light source is usually located as close to the camera as possible to take advantage of retroreflective targets at all facilities where the technique is used except for the NTF. At the NTF, where stringent model surface finish requirements preclude the use of retroreflective targets, test-section lights are used for diffuse illumination of polished paint targets. For measurements at the NTF, the camera is positioned to the side and somewhat above the model, resulting in an oblique view of the model. A target row is typically placed on or near the fuselage to serve as control, with additional target rows located at known semispan locations along the wing. Image processing is used to locate automatically and compute corrected image plane coordinates for each of the targets. Single-view photogrammetry is then used to determine the X (streamwise) and Z (vertical) coordinates in object space, given the known Y (crossflow) coordinates. Vertical displacements at specified chordwise locations and slope angles are computed by linear least squares for each semispan station along the wing.[5]

Facility

The NTF is a fan-driven, closed-circuit, continuous-flow, pressurized wind tunnel.[7] The $8.2 \times 8.2 \times 25$ ft-long test section has a slotted-wall configuration. However, for the test described here, the slots were covered. The wind tunnel can operate in an elevated temperature mode up to $T = 140°$F, normally using air and, in a cryogenic mode, using liquid nitrogen as a coolant, to obtain a test temperature range down to about $-250°$F. (However, note that for the test described here, the NTF was operated in air mode only at 95°F.) Thermal insulation inside the pressure shell minimizes energy consumption. The design total pressure range for the NTF is from 15 to 130 psia. The combination of pressure and cold test gas can provide a maximum Reynolds number of 1.2×10^8 at Mach 1.0, based on a chord length of 0.82 ft. These characteristics afford full-scale Reynolds number testing for a wide range of aircraft. Three types of investigations are possible: Reynolds number effects at constant Mach number and dynamic pressure, model aeroelastic effects at constant Reynolds number and Mach number, and Mach number effects at constant dynamic pressure and Reynolds number.

The constraints imposed by operation in a high-pressure environment over such a wide range of temperatures have had a significant impact on the continuing development, improvement, and optimization of instrumentation at the facility. A major instrumentation challenge at the NTF is the requirement to make measurements over the wide range of temperature from 140°F down to $-250°$F. Aeroelastic deformation measurements have been made at the NTF for both high-speed research and advanced subsonic technology full-span models. In all cases before the test described here, the emphasis of the aeroelastic measurements at the NTF was on the determination of the change in main element wing twist due to aerodynamic loading.[5] The results presented here represent the first attempt at the NTF to make aeroelastic measurements on a semispan model and the first attempt to measure the aeroelastics of components in addition to the main wing element.

Wind-Tunnel Test

The first test involving the measurements of TEF and shroud geometry at the NTF was conducted on a large representative military semispan steel wing during an air mode test at constant Mach number and varying dynamic pressures. Figure 1 illustrates the definition of gap as the distance from the trailing edge of the shroud to a tangent point on the TEF. Overhang is defined as the distance parallel to the model chordline from the trailing edge of the shroud to the leading edge of the TEF. The gap and overhang were adjusted using shim plates and serrated teeth, respectively, during model configuration changes. The gap was variable from 0.5 to 2.5%c and overhang was variable from -1.0 to 5.0%c in increments of 0.5%c.

Figure 2 depicts the entire semispan model with leading-edge flap (LEF), shroud, TEF, and standoff with labyrinth seal. The labyrinth seal and standoff plate were used to mitigate the effect of the

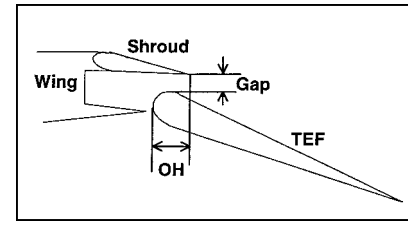

Fig. 1 Shroud, TEF, gap, and overhang (OH).

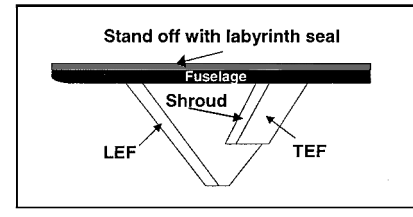

Fig. 2 Diamond wing high-lift model (top view).

wind-tunnel boundary layer on the aerodynamic performance. Uniformly distributed static loads applied pretest to the wing and shroud indicated relatively stiff wing components with little expected deformation. The air mode test served as an effective means to investigate implementation issues associated with the aeroelastic measurement technique and to evaluate the resolution of the measurement technique, while avoiding the complications that cryogenic operations introduce for optical instrumentation. The semispan wing was tested under the auspices of the Technical Cooperation Program, a multinational test program that includes NASA, Defense Evaluation and Research Agency (DERA) U.K., and the U.S. Navy. For this test the angle-of-attack range was from −5 to 24 deg, the Mach number fixed at 0.2 for the VMD runs, and the dynamic pressure range was from 60 to 350 psf (Reynolds numbers from 1.4×10^6 to 7.7×10^6/ft). Parametric studies were conducted on gap and overhang to determine the optimum settings for a configuration with specific angle settings for the shroud and TEF. In addition to studying the basic flow physics of military high-lift configurations, the test was also conducted for CFD validation.[8] Results from the test will be used as a benchmark for future CFD studies to predict high-lift system performance and, ultimately, high-lift system design. As such, it is critical to gauge the extent of deflection of the high-lift system under load. The components of the high-lift system (TEF and shroud) act as cantilever beams, which, under aerodynamic loading, may deflect. Because the gap between the TEF and the shroud was crucial to the parametric study during the test and is a main parameter for CFD studies, knowledge of the deformation is crucial.

Pretest Loading of Components

To estimate the potential deflection due to aerodynamic loading before testing, static loading tests were conducted. The shroud was uniformly loaded using weighted bags and the TEF was loaded with point loads attached to the flap ends near the one-quarter chord. With the shroud set to a deflection angle of 23 deg and the TEF set to 35 deg (23/35 configuration), a load of 420 lb applied to the TEF was found to decrease the gap a maximum of 0.008 in. measured at the bracket location. The shroud, loaded to 20 lb was found to increase the gap 0.0045 in. Therefore, a pretest estimate of the maximum change in gap was established as the difference between these readings to be on the order of 0.0035 in. In the worse case, with zero shims corresponding to a gap of 0.196 in. (or 0.5% of the undeflected wing chord located at the midspan of the flap), this estimated deflection would be 1.8% of the unloaded gap.

Optical Target Layout and Application

The special illumination technique developed for full-span models at the NTF involves the imaging of a black test-section wall as seen in reflection from the mirrorlike wing surface.[5] In such cases, good contrast targets are possible with an application of polished-paint white dots on the wing and fuselage without any additional background painting required. A similar illumination technique has not yet been perfected for semispan testing. Thus, to ensure reasonable contrast targets, white dots on a black background were used for this first semispan test. The targets consisted of polished-paint white dots of 0.5-in. diameter on a black background several diameters wide. The locations of the targets were chosen to minimize interference with pressure taps and were generally located away from taps or centered between pressure tap rows. The targets were positioned with aid of precision metal-foil templates that facilitated the target application to model parts that would be used later in the test, especially in one case in which half of two targets would be replaced during a configuration change. The use of precision templates to locate the targets was especially useful because over 90 configuration changes were anticipated for the test. The templates also facilitated the determination of the semispan (Y coordinate) of each target for entry into data-reduction setup files. All layout, painting, and polishing of the targets was accomplished in a ready bay preparation site before the model was moved to the test section.

The application procedure began with a chemical cleaning of the model to remove any residual oil or film that might hamper adhesion of the paint, which was the standard basecoat typically used for pressure sensitive paint (PSP) applications. The circular targets were then masked at the proper locations and painted with an air gun. The masking was removed after an hour or so of drying under infrared illumination (used to decrease paint drying time). The masks for the black background were then applied and the black paint applied over the white targets. After drying, the targets and backgrounds were polished with 2000 grit paper and water to yield a final typical thickness of 0.0005 in. and a surface roughness of less than 10 μin. as verified by measurements with thickness and roughness gauges. The height of the paint was estimated to have no aerodynamic effect based on estimates of detrimental aerodynamic step height given in Ref. 9.

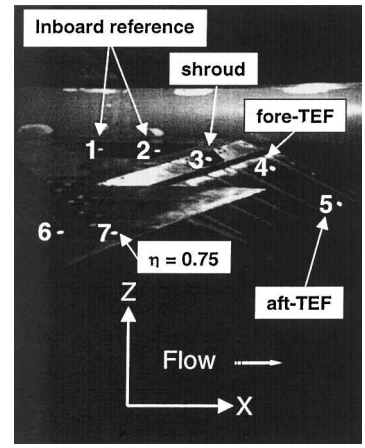

Fig. 3 Model and targets viewed from camera.

Two targets were located near the wing root where deformation was expected to be minimized. The wing-root targets were used as a reference for computation of the deformation due to aerodynamic loading. Two targets were also placed in a row at a normalized semispan η, equal to 0.75, to determine the change in twist of the main wing element. Targets were placed on the shroud and near the leading and trailing edges of the TEF. The painted targets with black background can be seen in Fig. 3 on the TEF and shroud. The root reference target row can be seen at the top of Fig. 3. This image is from the camera used to make the model deformation measurements with targets and coordinate system labeled.

Camera Setup and Lighting

The CCD video camera must be protected from extremes in the operating environment. Temperature and humidity operating requirements for the camera are from 0 to 40°C, with a relative humidity of from 50 to 70%. Environmentally protected pressure housings that can supply heating or cooling are used at the NTF for the VMD cameras due to the large temperature and pressure excursions at the facility. Tests at the NTF have shown that, when possible, it is generally advantageous to mount the camera with a fixed mount rather than with a pan-tilt unit that may be subject to movement under flow conditions. The interline transfer CCD camera used for this test was an instrumentation-grade video-rate camera with a resolution in interlaced mode of 768 pixels horizontal by 493 pixels vertical. The horizontal and vertical pixel spacings are 11.0 and 13.0 μm, respectively. The target-tracking VMD measurement system digitizes the video image to a resolution of 640 by 480 pixels. A zoom lens was used at a focal setting selected to capture properly the targets of interest throughout the expected pitch range of the test. Standard test-section lighting, also used for surveillance while testing, was used to illuminate the targets. The search for a combination of test-section lights to yield suitable contrast over the entire pitch range was the most time-consuming activity during setup. Often, the lighting settings sufficient for reasonable contrast at a given pitch angle would be unsuitable for other pitch angles. A compromise in the lighting was finally found that could work over the entire pitch range while still allowing sufficient illumination for the test-section surveillance cameras that are required to be operational during testing.

Data Acquisition System

This was the first test at the NTF in which the target-tracking system developed by the High Technology Corporation (HTC) under NASA contract[4] was used as the primary data-acquisition system for model deformation measurements. For previous tests at the NTF, all of which were full-span models, an in-house developed automated image acquisition and reduction system had been used.[5] The in-house developed system works well for scenes in which the targets stand out from the background significantly, such as occurs with the special illumination and targeting technique developed for the NTF discussed earlier. In cases where additional glints or spots on the model might be interpreted as false targets, the in-house system may fail. Because the HTC tracking system tracks individually designated targets (by mouse or by selection of a previous centroid file) continuously at a 15-Hz rate, any glints or false targets that are more than a few target diameters away from the true targets will not perturb the data acquisition. Because the quality of the images was expected to be significantly degraded from that possible with full-span models, the HTC system was selected for primary data acquisition for the model deformation measurements. A number of potential false targets and glints can be seen in Fig. 3 that would have been very troublesome for the in-house developed system.

A major difference between the HTC tracking system and the in-house developed system is that the HTC system tracks targets and outputs centroid files on trigger while the acquisition program is running, but does not do any additional reduction except for a limited quick look capability. On the other hand, the in-house developed system automatically finds targets, locates centroids, sorts targets, correlates data with facility point number, determines the change in wing twist as each data point is taken, and outputs the reduced data to files. Because the final reduction can not be accomplished until the end of a set of runs for the HTC system, the data turnaround time is increased from that experienced for full-span models when using the in-house developed deformation measurement system. Thus, the model deformation data may be transferred to the customer as a separate data file, instead of being merged with the rest of the data shortly after a run series as for full-span testing. However, the improved robustness of the HTC tracking system for this semispan model proved worth this tradeoff.

System Calibration

The measurement system was calibrated with a three-step process. First, the camera was calibrated for lens distortion. The location and pointing angles of the camera were then determined in the test-section coordinate system. Finally, angles and (X, Z) coordinates were referenced to a wind-off polar (an alpha sweep over the same pitch range as for a wind-on polar).[5] Figure 4 shows an image from the data camera during the first step. During this phase a calibration fixture consisting of a three-stepped plate with targets at known locations is positioned to occupy as much of the field of view as possible. A centroid file is then recorded from which several camera parameters associated with imaging and needed for the photogrammetric reduction are recovered. The new camera parameters are then used in the subsequent step of the calibration. For the second calibration step, the three-step calibration plate is aligned to the test section coordinate system so that X is in the flow direction, Z is up, and Y is along the span direction defined by the right-hand rule (Fig. 5). It is the Y value that serves as the known input to enable computations of X and Z with a single camera. A row of pressure taps near the root was used to align the calibration plate in the streamwise direction. A precision bubble level was used to establish parallelism to the Y axis, which is assumed to be horizontal. It is not necessary to level the plate in the pitch direction (rotation about the Y axis) because the offset in pitch is determined by wind-off polars used for final system calibration. The orientation parameters in the test-section coordinate system were then input into a data-reduction setup file. As a check of the first two steps in calibration and to ensure that the system and setup files are established correctly, the difference in the computed X coordinates of targets at the inboard row and outboard row were compared to ensure agreement to their known values based on measurements during target layout.

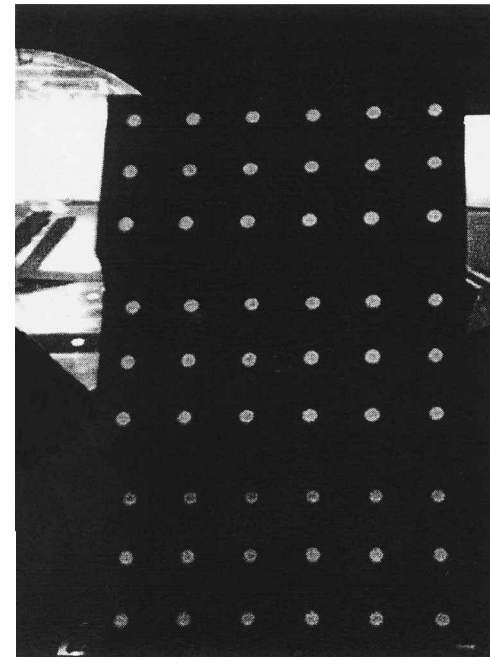

Fig. 4 View from data camera with three-stepped plate positioned for determining camera calibration parameters.

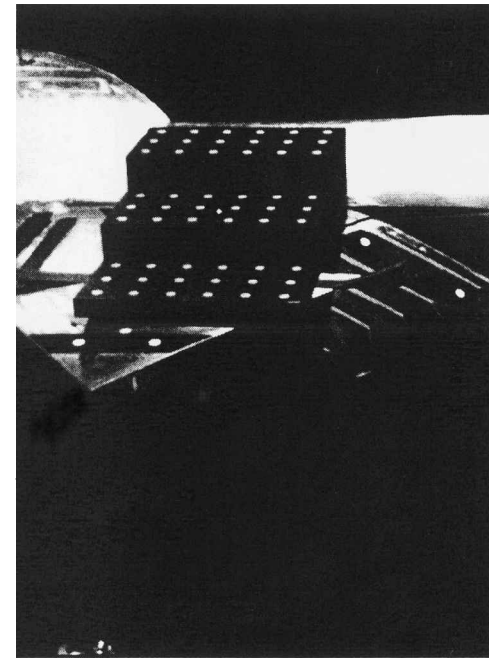

Fig. 5 View from data camera with three-stepped plate positioned for determining camera orientation in test-section coordinate system.

The third calibration step begins with a wind-off polar at, or near, the total temperature and pressure at which flow data will be taken. A third- to fifth-order polynomial least-squares fit is used to establish correction coefficients based on the onboard accelerometer used to determine the pitch angle of the model. The correction coefficients force the angles measured by the VMD measurement system to agree with the onboard accelerometer and account for slight zero shifts and changes in system response as a function of time or tunnel conditions. The use of wind-off polars may not be as crucial when conducting tests in air mode such as for this test, but is especially critical when in cryogenic mode due to the larger temperature excursions that are possible with associated mounting structure movement. For this test the wind-off polars were also used to establish the motion in the X–Z plane under wind-off conditions. The X–Z wind-off value at a given alpha (based on the polynomial curve fit) can then be interpolated and subtracted from the flow data to yield differences from wind-off to wind-on.

Data Acquisition and Reduction

A transistor–transistor-logic trigger from the facility data-acquisition system (DAS) automatically initiated data acquisition. On trigger, the centroids of the next 75 images (representing 5 s of image acquisition) were recorded to a data file with a sequential VMD point number that was independent of the DAS point number. After the centroid file is stored, a file prepared by DAS containing point number, run number, Mach, alpha, and several other tunnel parameters is retrieved from a shared drive to create a log file with DAS data correlated with VMD point numbers for later reductions.

At the conclusion of a set of runs, data reduction is initiated by selecting inclusive VMD point numbers for the runs that need to be reduced, with the wind-off run(s) and wind-on runs discriminated. MATLAB® scripts are then used for further reductions. The data-reduction operations include the following. Centroid coordinates in pixel units are converted to millimeters units based on horizontal and vertical pixel spacings. The distortion correction parameters found in step 1 of the calibration procedure are then applied for use in the single-camera, single-view photogrammetric determinations of X and Z target coordinates based on known Y coordinates from setup files. Angle computations in an (X, Z) coordinate plane are then made for targets identified as constituting a given row. Polynomial coefficients are determined based on the wind-off polar(s) for application to the wind-on data to determine the difference between wind-off and wind-on for angles and X and Z coordinates. For the aeroelastic twist computation at $\eta = 0.75$, the angle of the inboard row of targets near the root of the main wing element was used as reference and subtracted.

In full-span testing, sting bending causes a displacement of the model during flow. Thus, at a given alpha, the model position with and without flow may differ, requiring the use of a target row on the body as reference to remove any apparent twist of the body. For semispan testing it was assumed originally that a direct subtraction of interpolated X and Z values from the wind-off reference polar would be the best procedure. However, it was found that in some cases displacements (real or apparent) between wind-off and wind-on data were actually larger than the relatively small deformation due to aerodynamic loading. Vector displacements from wind-off to wind-on for one of the high-Q runs are presented in Fig. 6 for targets 1–5, with the target numbers indicated above each arc (caused by the alpha sweep during the polar from −5 to 24 deg). The similarity of the displacement vectors for the five targets indicates rigid-body motion. Targets 1 and 2 were located on the very rigid inboard portion of the main wing element, where it is reasonable to assume no deformation between wind-off and wind-on. However, significant displacements were recorded (either real rigid-body displacements or an artifact of the measurement process) that must be removed to determine properly the deformation of the shroud and TEF.

Several methods were investigated to eliminate or reduce the apparent displacement of the inboard targets from wind-off to wind-on. These methods included the subtraction of interpolated (from polynomial fits) X and Z values of just target 2. (Interpolation of wind-off data is necessary because the wind-on data may not be at the precise

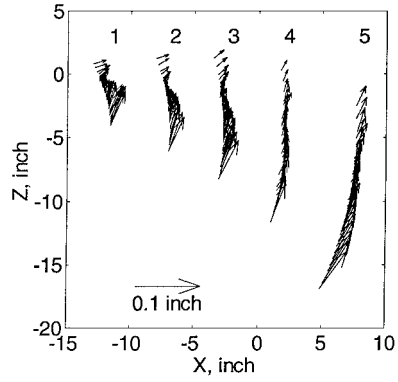

Fig. 6 Vector displacements from wind-off to wind-on for a high-Q run without compensation; target numbers are indicated.

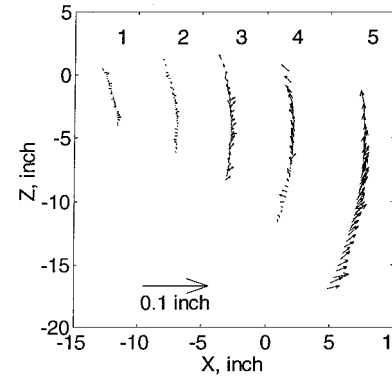

Fig. 7 Vector displacements from wind-off to wind-on for a high-Q run with compensation; target numbers are indicated.

settings used for the wind-off polar). A second method involved the use of a conformal transformation via nonlinear least squares using targets 1 and 2 from the wind-off polar (again from polynomial fits) as reference to yield a pitch correction angle and translations in X and Z. However, the angle computed using the conformal transformation was found to have errors in alpha that were 2–5 times larger than the estimated uncertainty of the precision servoaccelerometer used to measure alpha. Thus, a compromise was made and the means of the interpolated displacements in X and Z of targets 1 and 2 determined from the corresponding wind-off polar were subtracted from the wind-on polar to arrive at the final displacement.

Displacement vectors for the run of Fig. 6 reduced in this manner are plotted in Fig. 7 at the same scale as Fig. 6 for comparison. For Fig. 7, most of the apparent rigid-body bias is removed, leaving the wind-off to wind-on deformation. The displacement vectors for targets 1 and 2 on the inboard portion of the main element of the wing serve as a measure of the noise of the measurement process.

ΔX was computed as

$$\Delta X_n = (X - X_o)_n - [(X - X_o)_1 + (X - X_o)_2]/2 \tag{1}$$

where $n = 3, 4$, or 5 represents the target number on the shroud, fore TEF, and aft TEF, respectively; o represents interpolated wind-off X values from the polynomial fit as a function of model alpha; and X without a subscript represents X data from the wind-on polar. A similar expression applied for ΔZ:

$$\Delta Z_n = (Z - Z_o)_n - [(Z - Z_o)_1 + (Z - Z_o)_2]/2 \tag{2}$$

The displacement magnitude in X and Z, denoted by L_n, was then found from

$$L_n = \sqrt{(\Delta X_n)^2 + (\Delta Z_n)^2} \tag{3}$$

The angle ϕ_n of the displacement vector was also computed as

$$\phi_n = \tan^{-1}(\Delta Z_n / \Delta X_n) \tag{4}$$

The order of the signs of the ΔX and the ΔZ terms was used to determine the four quadrant inverse tangent with a range of ±180 deg (atan2[$\Delta Z, \Delta X$] function in MATLAB). With this sign convention, positive angles are found for displacements in the positive Z direction and negative angles are found for displacements in the negative Z direction.

Δgap due to aerodynamic loading is approximated by

$$\Delta\text{gap} = \frac{\Delta Z_3 - \Delta Z_4}{\cos\alpha} \tag{5}$$

where α is the geometric angle of attack of the semispan model. The approximation to the change in gap can also be described in terms of the displacement magnitude and vector angle as

$$\Delta\text{gap} = \frac{L_3 \sin\phi_3 - L_4 \sin\phi_4}{\cos\alpha} \tag{6}$$

Likewise, ΔOH due to aerodynamic loading is approximated by

$$\Delta\text{OH} = \frac{\Delta X_4 - \Delta X_3}{\cos\alpha} \tag{7}$$

The corresponding relation in terms of the magnitude and angle of the displacement vector for the change in overhang is given by

$$\Delta\text{OH} = \frac{L_4 \cos\phi_4 - L_3 \cos\phi_3}{\cos\alpha} \tag{8}$$

Representative Data

Model deformation measurements were not made throughout the test, but rather for selected data sets ($\sim$110 runs). All data were taken at Mach 0.2 in air mode at three dynamic pressures of 63.5, 170.9, and 347.5 psf, corresponding to total pressures of 16.2, 43.5, and 88.2 psf. The total temperature was 95°F for all runs. The angle-of-attack range was from -5 to 24 deg. Wind-off reference polars were generally made at pressures of 16.2 and 88.2 psf at the beginning and end of a run series with the 16.2 psf pressure polar used to reduce the 43.5 psf runs. The 43.5 psi runs are, thus, subject to more error compared to the other pressures.

Displacement vectors for low-Q (63.5 psf) and high-Q (347.5 psf) runs are presented in Figs. 8 and 9, respectively. (The run presented in Fig. 9 is the same run used to illustrate the data reduction procedures in Figs. 6 and 7, but with an increased scale factor of 3.3 times for the displacement.) For Figs. 8 and 9, the displacement vectors of targets 1 and 2 serve as a measure of the noise level for the measurement process. For the low-Q run of Fig. 8, the deformation (except for target 5 on the aft TEF) is generally within the noise level of targets 1 and 2. The increased displacements for the high-Q run are obvious, as is an increase in the noise level. The aft TEF is seen to deflect generally in a direction influenced by the direction of the aerodynamic loading, with a net reduction in the flap angle. The shroud experiences similar behavior, but with less magnitude and more relative data scatter. The fore-TEF target number 4 actually appears to deflect toward the shroud, which would be consistent with a rotation of the TEF in an upward sense ($+Z$ direction) with the hinge line located below target 4.

The change in twist θ_2 (in degrees) due to aerodynamic loading at a normalized semispan of $\eta = 0.75$ is plotted vs alpha in Fig. 10 for each of three dynamic pressures. The low- and high-Q runs are the same runs as plotted in Figs. 8 and 9. Little direct dependence on Q is noted and a relatively small amount of twist is indicated. Hence, it is assumed that the values shown in Fig. 10 are more indicative of the noise level for the twist measurement and serve as an upper bound of the twist likely experienced at the $\eta = 0.75$ semispan station. Note that 0.05 deg scatter in the twist data corresponds to 0.0035-in. scatter in displacement for the targets, which are separated by 4 in.

The magnitudes of the displacements L_n are plotted vs alpha in Fig. 11 for low-, medium-, and high-Q runs. The shroud

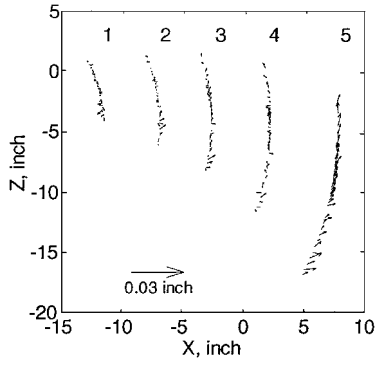

Fig. 8 Vector displacements from wind-off to wind-on for a low-Q run (63.5 psf); target numbers are indicated.

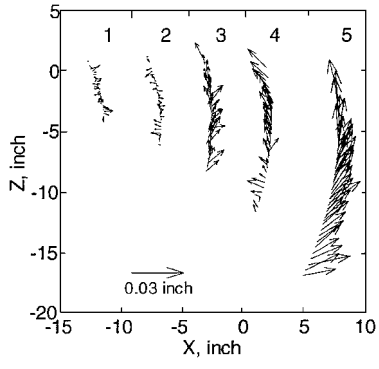

Fig. 9 Vector displacements from wind-off to wind-on for a high-Q run (347.5 psf); target numbers are indicated.

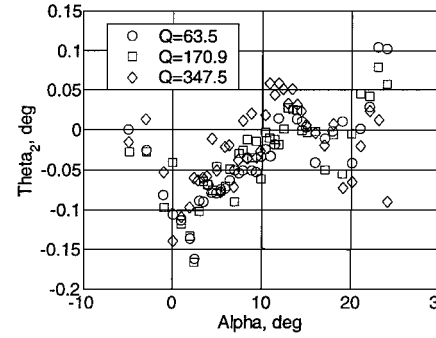

Fig. 10 Aerodynamically induced twist θ_2 for three dynamic pressures Q (pounds per square foot).

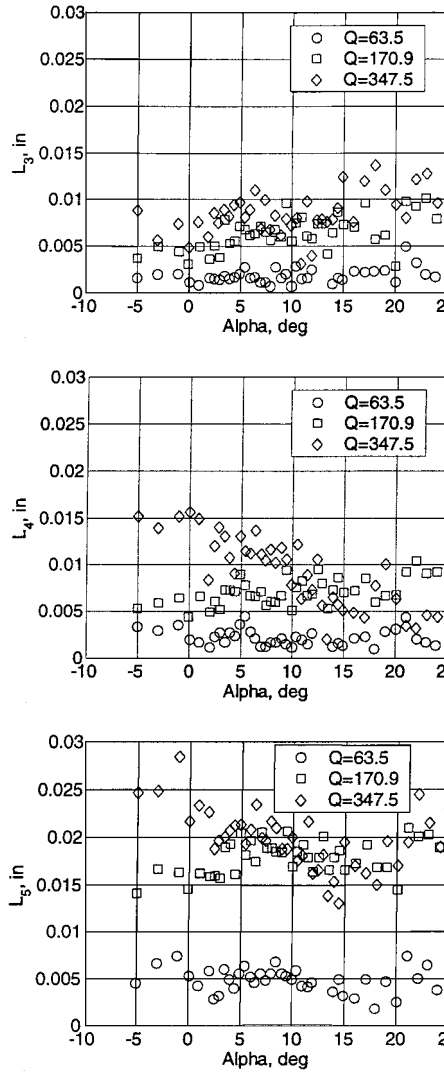

Fig. 11 Magnitude of the displacement for a) shroud, b) fore TEF, and c) aft TEF for three dynamic pressures Q (pounds per square foot).

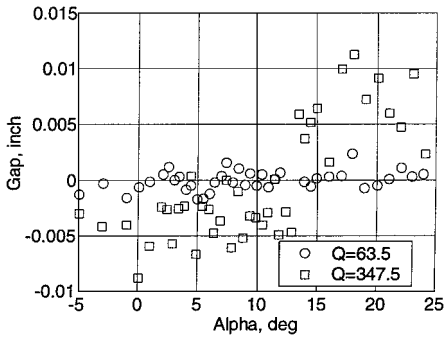

Fig. 12 Change in gap induced by aerodynamic loading for low and high dynamic pressure Q (pounds per square foot) vs alpha.

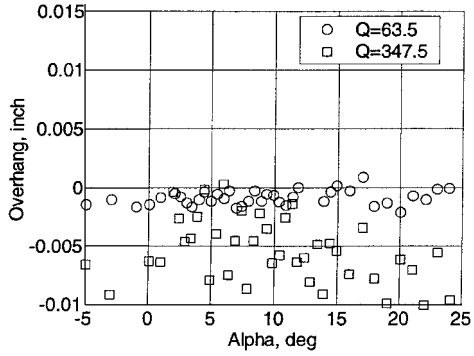

Fig. 13 Change in overhang induced by aerodynamic loading for low and high dynamic pressure Q (pounds per square foot) vs alpha.

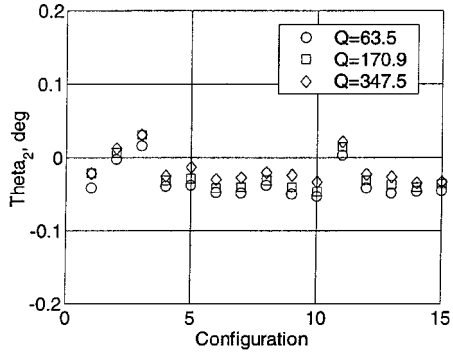

Fig. 14 Aerodynamically induced twist θ_2 for three dynamic pressures Q (pounds per square foot) vs configuration number.

displacement L_3, with the least magnitude of the data plotted, has a definite dependence on the dynamic pressure. At the lowest Q (63.5 psf), the magnitude of the displacement of the shroud, Fig. 11a, is generally less than 0.003 in. and probably represents the noise level of the measurement system for such measurements. At the highest Q (347.5 psf), the magnitude of the displacement is generally less than 0.01 in., except at high alpha. A similar behavior is noted for the fore-TEF target, Fig. 11b, except that the high-Q data tends to decrease with alpha. The aft-TEF data, Fig. 11c, exceeds considerably the shroud and fore-TEF data and shows little dependence on alpha. The magnitude of the displacement of the aft TEF approaches 0.03 in. for the high-Q run. The corresponding changes in gap and overhang are plotted vs alpha in Figs. 12 and 13 for the same low- and high-Q runs of Fig. 11.

Data for 15 configurations, during which model deformation measurements were made, are summarized in Figs. 14 and 15. Mean values for all alphas are plotted vs configuration number, to yield a sense of the deformation for a large block of the data set. Data are presented for low-, medium-, and high-Q runs. The change in twist data θ_2, plotted in Fig. 14, indicates a noise level for aerodynamically induced twist of about 0.05 deg, showing little dependence on

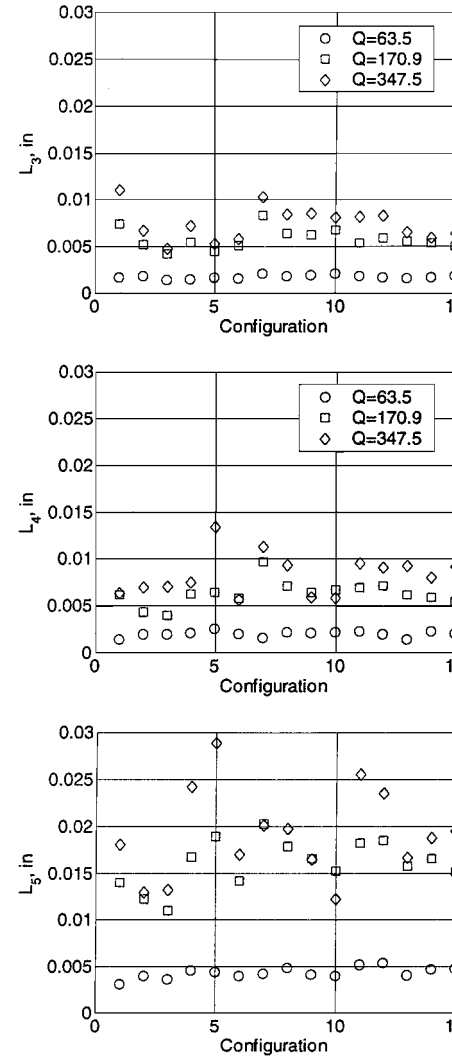

Fig. 15 Magnitude of the displacement for a) shroud, b) fore TEF, and c) aft TEF for three dynamic pressures Q (pounds per square foot) vs configuration number.

configuration. The displacement magnitude plots of Fig. 15 show a clear dependence on Q, but little dependence on configuration.

Uncertainty

The VMD measurement system resolution depends on the fraction of the image field that the targets occupy. For cases in which the row of targets span nearly the entire image plane, resolution better than 0.01 deg is possible in the laboratory. Wind-tunnel angle-of-attack tests using body targets indicate that 0.01-deg resolution can be achieved during wind-off tests and may be possible for wind-on tests, provided that the target row(s) occupy nearly the entire image plane and that model translations while changing pitch are not excessive. However, the fraction of the image plane occupied by targets for the test described here is closer to 30% to image all segments simultaneously, reducing the resolution considerably from what is possible in a controlled laboratory situation. The targets are also displaced from the center of rotation, especially the aft-TEF target, producing relatively large translations in the image plane when pitching the model. The large translations and being located near the edge of the image plane make the measured target locations more susceptible to residual image plane distortion. For similar reasons, the displacement measurement precision for this test is of the order of 0.003 in. compared to the 0.0001-in. precision that can be achieved during controlled laboratory experiments.

A change from the standard procedures used for full-span models was implemented in which the tunnel alpha was used to determine the correction data from the wind-off curve fit rather than

the reference inboard pitch angle determined from VMD measurements. For full-span models, where the change in twist is the primary measurement and model dynamics can corrupt the onboard accelerometer readings, it has been determined the best practice to use the VMD measured reference angle (usually from targets on the fuselage) instead of tunnel alpha. However, for semispan testing, the accelerometer is generally subjected to less dynamic oscillations, reducing that potential error source. In addition, for situations in which spatial as well as angular data are required, it is advantageous to use the tunnel alpha as reference when the targets are displaced from the center of rotation of the model. In such cases, small errors in the reference angle may lead to errors in displacement that are comparable to those due to deformation. For instance, for a target that is displaced from the center of rotation by 30 in., an error of 0.01 deg causes as error of approximately 30 in. $\times$ 0.17 m, or 0.005 in. in the displacement.

Conclusions

During this first use of the videogrammetric deformation measurement technique for semispan component testing at the NTF, apparent rigid-body motion between the wind-off and wind-on polars was larger than expected. Of the several methods investigated to alleviate this problem, a simple method of removing the mean displacement of the inboard main-wing-element targets was adopted. As an overall summary, the deformation data were found to be somewhat independent of configuration with little alpha dependence except for the aft TEF. The aerodynamically induced twist was found to be less than 0.1 deg overall, which is considered to be the noise floor of the optical measurements for the setup for this test. The noise floor for displacement measurements was found to be about 0.003 in. The VMD measurement technique was determined to be an effective way of determining component deformation, or at least to establish limits of the deformation during semispan testing.

Acknowledgments

Luke A. Catella is acknowledged for his innovations in target layout and polished paint application. Harriett Dismond and Kenneth Cate are acknowledged for continuing support in videogrammetric model deformation installations, calibration, and operations. The operations and research staff at the NASA Langley Research Center National Transonic Facility are acknowledged for assistance and support in the aeroelastic measurements phase of this test.

References

[1]Burner, A. W., Snow, W. L., and Goad, W. K., "Model Deformation Measurements at a Cryogenic Wind Tunnel Using Photogrammetry," *Instrumentation in the Aerospace Industry*, Instrument Society of America, Pittsburgh, PA, Vol. 31, 1985, pp. 615–622.

[2]Brooks, J. D., and Beamish, J. K., "Measurement of Model Aeroelastic Deformations in the Wind Tunnel at Transonic Speeds Using Stereophotogrammetry," NASA TP 1010, Oct. 1977.

[3]Burner, A. W., and Martinson, S. D., "Automated Wing Twist and Bending Measurements Under Aerodynamic Load (Invited)," AIAA Paper 96-2253, June 1996.

[4]Liu, T., Radeztsky, R., Garg, S., and Cattafesta, L., "Videogrametric Model Deformation System and Its Integration with Pressure Paint," AIAA Paper 99-0568, Jan. 1999.

[5]Burner, A. W., "Model Deformation Measurements at NASA Langley Research Center," *Symposium on Advanced Aerodynamic Measurement Technology*, CP-601, AGARD, 1998, pp. 34-1–34-9.

[6]Burner, A. W., Liu, T., Garg, S., Bell, J. H., and Morgan, D. G., "Unified Model Deformation and Flow Transition Measurements," *Journal of Aircraft*, Vol. 36, No. 5, 1999, pp. 898–901.

[7]Hill, J. S., "National Transonic Facility," *Research and Technology Highlights*, NASA TM-4708, Dec 1995, pp. 122, 123.

[8]Ghee, T. A., and Taylor, N. J., "Low-Speed Wind-Tunnel Tests on a Diamond Wing High-Lift Configuration," AIAA Paper 2000-4507, Aug. 2000.

[9]Holmes, B. J., Obara, C. J., Martin, G. L., and Domack, C. S., "Manufacturing Requirements," *Proceedings on Laminar Flow Aircraft Certification*, NASA CP-2413 compiled by L. J. Williams, May 1986, pp. 171–183.